Desalination 274 (2011) 182–191

Contents lists available at ScienceDirect

Desalination

journal homepage: www.elsevier.com/locate/desal

# A combined pore blockage, osmotic pressure, and cake filtration model for crossflow nanofiltration of natural organic matter and inorganic salts

Supatpong Mattaraj [a,b,*], Chalor Jarusutthirak [c], Chareopon Charoensuk [a], Ratana Jiraratananon [d]

[a] Environmental Engineering Program, Department of Chemical Engineering, Faculty of Engineering, Ubon Ratchathani University, Ubonratchathani 34190, Thailand
[b] National Center of Excellence for Environmental and Hazardous Waste Management, Ubon Ratchathani University, Ubonratchathani 34190, Thailand
[c] Department of Chemistry, Faculty of Science, King Mongkut's Institute of Technology Ladkrabang, Bangkok 10520, Thailand
[d] Department of Chemical Engineering, Faculty of Engineering, King Mongkut's University of Technology Thonburi, Bangkok 10140, Thailand

ARTICLE INFO

*Article history:*
Received 3 November 2010
Received in revised form 1 February 2011
Accepted 5 February 2011
Available online 4 March 2011

*Keywords:*
Cake filtration
Inorganic salt
Nanofiltration
Natural organic matter
Osmotic pressure
Pore blockage

ABSTRACT

The performance of nanofiltration (NF) process for water treatment is affected by flux decline due to membrane fouling. Many models have been applied to explain fouling mechanisms. In this work, a combined pore blockage, osmotic pressure, and cake filtration model was developed and successfully used to determine NF performance and model parameters for crossflow NF. NOM solutions containing sparingly soluble inorganic salts (i.e. $CaCO_3$, $CaSO_4$, and $Ca_3(PO_4)_2$), showed higher normalized flux decline than those containing soluble inorganic salts (i.e. NaCl and $CaCl_2$). The $\alpha_{blocked}$ and $R_{m,s}$ parameters for sparingly soluble inorganic salts exhibited higher values than those for soluble inorganic salts, while the $R_{m,s}$ and $\alpha_{cake}$ parameters were found to be significant for soluble inorganic salts due to increased salt concentration and NOM cake accumulation at the membrane surface. Increased ionic strengths from 0.01 M to 0.11 M resulted in more pronounced flux decline, thus increased model parameters (i.e. $\alpha_{blocked}$ and $R_{m,s}$). The membrane surface characteristics examined by the scanning electron microscopy (SEM) images evidently supported the precipitation of sparingly soluble inorganic salts. The flux decline was the most pronounced for phosphate species, corresponding to the lowest water flux recovery, thus increased non-recoverable resistance ($R_{non\text{-}rec}$) due to pore plugging from phosphate salt precipitation.



## Introduction

Membrane processes have been increasingly used in the applications of drinking water treatment to meet more stringent water quality regulations [1]. Of particular interest is the use of nanofiltration (NF) to effectively remove dissolved natural organic matter (NOM) and simultaneously control disinfection by-products (DBPs) after chlorination process of drinking water treatment [2]. However, membrane fouling can significantly reduce membrane performance, thus increase operating costs due to higher operating pressures, and frequent chemical cleaning leading to shortened membrane life [3]. Fouling may be attributed to several mechanisms including concentration polarization of retained solutes, pore blocking by solutes adsorbed on the membrane surface and/or within pores, and cake layer formation, which presents an additional resistance to flow, and precipitation of inorganic, and organic solutes as a result of high concentration at the membrane surface [4,5].

Natural organic matter is considered as a major membrane foulant during NF [6]. NOM component comprises a heterogeneous mixture of organic materials with wide molecular size distribution and functional groups [7,8]. Membrane fouling caused by NOM can be dependent on molecular size distribution of feed solution components. Components smaller than membrane pores can penetrate the membrane pores, while larger components including aggregates can block membrane pores and contribute to cake formation [9]. Yuan and Zydney [10] indicated that both pore blockage and surface deposition can dominate fouling mechanisms of humic acid during ultrafiltration, when compared with adsorption and concentration polarization. The accumulation of retained dissolved organic matter (DOM) mass significantly affected membrane fouling, while larger pore membranes exhibited significant flux decline in comparison with smaller pore membranes [11]. Jurusuthirak et al. [12] exhibited that cake formation dominated permeate flux decline with increased NOM concentration.

Inorganic fouling is one of the major limitations of NF applications in drinking water treatment [13,14]. This fouling is induced by concentration polarization and scale formation (or precipitation fouling) during NF. An increased concentration of the scale-forming species in the bulk solution occurs due to permeate withdrawal, which is further enhanced in the region next to the membrane surface

* Corresponding author at: Department of Chemical Engineering, Faculty of Engineering, Ubon Ratchathani University, Warinchumrab, Ubonratchathani 34190, Thailand. Tel.: +66 45 353 344; fax. +66 45 353 333.
*E-mail addresses:* supatpong.m@hotmail.com, mattas@ubu.ac.th (S. Mattaraj).

0011-9164/$ – see front matter © 2011 Elsevier B.V. All rights reserved.
doi:10.1016/j.desal.2011.02.010

by the superimposed effect of concentration polarization [15]. Flux decline caused by inorganic fouling is dependent on solution pH, ionic strength and solution types [16,17]. It was evident that an increase of NaCl concentration or the presence of divalent cations increased osmotic pressure due to high salt concentration [12] and enhanced membrane membrane fouling [17]. Multivalent cations can lead to more membrane fouling when combined with polyanions, such as carbonate ($CO_3^{2-}$), sulphate ($SO_4^{2-}$), and phosphate ($PO_4^{3-}$) ions, thus attributing to pore blockage of precipitated species formed and blocked membrane surface and/or pores [15,18]. However, the influence of combined inorganic salts and NOM with different solution chemistry during NF fouling is required to understand fouling mechanisms in order to mitigate membrane fouling.

In our previous work [19], a combined osmotic pressure and cake filtration model for crossflow nanofiltration of NOM was proposed. This model integrates the combined effects of osmotic pressure caused by retained salt concentration in the boundary layer of the membrane surface and cake formation caused by additional NOM cake resistance. The model can be used successfully to interpret membrane performances during crossflow NF of soluble inorganic salt with NOM. In addition, the model parameters due to the effect of operating conditions in crossflow reverse osmosis can be successfully evaluated [20]. However, we could not apply this model for solutions containing sparingly soluble inorganic salts with NOM due to different fouling mechanisms observed [18]. Therefore, this paper describes the modified mathematical fouling model, which combines pore blockage, osmotic pressure, and cake filtration model for crossflow NF of NOM with the presence of different inorganic salts. The objective of this study was to determine nanofiltration performance and model parameters of the modified mathematical fouling models. The results of this work also include the changes in the model parameters with different inorganic salts (i.e. $Cl^-$, $CO_3^{2-}$, $SO_4^{2-}$, and $PO_4^{3-}$) and ionic strengths (I.S.) of different multivalent cations (i.e. calcium and magnesium). The membrane performance and model parameters were estimated to provide an insight of fouling phenomena during NF of NOM and salts. Membrane surface characteristics were examined by scanning electron microscope (SEM) in order to illustrate surface images of the fouled membrane surface.

## 2. Theory

### 2.1. Solution flux

Solution flux during membrane filtration can be determined in terms of membrane permeability and the net transmembrane pressure gradient ($\Delta P - \sigma\Delta\pi$)as follows [19]:

$$J_v = L_p(\Delta P - \sigma\Delta\pi) = \frac{\Delta P - \sigma\Delta\pi}{\mu(R_m + R_{non-rec})} \quad (1)$$

where $J_v$ is the solution flux ($Lm^{-2}h^{-1}$, LMH); $L_p$ is the membrane permeability (LMH $kPa^{-1}$), $\Delta P$ is the averaged transmembrane pressure (kPa); $\sigma$ is the osmotic reflection coefficient (estimated by the intrinsic membrane rejection; ($R_{mem} = 1 - C_{perm}/C_{mem}$); $C_{mem}$ and $C_{perm}$ are the solute concentrations at the membrane surface and in the permeate (mol $L^{-1}$); $\Delta\pi$ is the difference in osmotic pressure of the solution at the membrane ($\pi_{mem}$) and in the permeate ($\pi_{perm}$), $\Delta\pi = \pi_{mem} - \pi_{perm}$ (kPa); $\mu$ is the dynamic viscosity (kg $m^{-1}s^{-1}$); $R_m$ is the membrane hydraulic resistance ($m^{-1}$); $R_{non\text{-}rec}$ is the additional resistance due to the non-recoverable resistance ($m^{-1}$). For clean water flux ($J_{vo}$), solution flux can be evaluated for unfouled membrane, while the effects of osmotic pressure and non-recoverable resistance are relatively small and therefore neglected. Membrane hydraulic resistance can be described by the Hagen-Poiseuille equation for laminar flow in the assumption of a uniform membrane pore radius ($r_p$) (m), while clean water flux can be written as follows:

$$J_{vo} = \frac{\Delta P}{\mu R_m} = \frac{N\pi r_p^4 \Delta P}{8\mu\delta_m} \quad (2)$$

where $N$ is the number of pores per unit membrane area (pores $m^{-2}$); and $\delta_m$ is the membrane thickness (m).

### 2.2. Pore blockage model

Pore blockage model illustrates the rate of change in the number of pores (or pore area,$A_{p,T} = NA_m\pi r_p^2$), which can be assumed to be proportional to the net transport of solute to the membrane surface [21].

$$\frac{dA_{p,T}}{dt} = \pi r_p^2 A_m \frac{dN}{dt} = -\alpha_{blocked} A_m C_{reten,NOM}(t)(J_{vo} - J^*) \quad (3)$$

where $A_m$ is total active permeable membrane area ($m^2$); $t$ is the operating period (min); $\alpha_{blocked}$ is the pore blockage efficiency ($m^2\,kg^{-1}$); $C_{reten,NOM}$ is the NOM concentration in the retentate (kg $m^{-3}$), which can be determined based on the mass balance model [19]; $J^*$ is the effective flux associated with back-transport resulting from crossflow (LMH). Eqs. (1), (2), and (3) can yield Eqs. (4) and (5), which describe the pore blockage model:

$$\frac{dJ_v}{J_{vo}dt} = \frac{dA_p}{A_m dt} \quad (4)$$

$$\frac{dJ_v}{dt} = -\alpha_{blocked} C_{reten,NOM}(t) J_{vo}(J_{vo} - J^*). \quad (5)$$

### 2.3. Combined osmotic pressure and cake filtration model

The combined osmotic pressure and cake filtration model was developed to evaluate nanofiltration performance of a solution containing both salt and NOM [19]. This model incorporates additional term of cake resistance ($R_c$), which is used to characterize flux in ultrafiltration and microfiltration [22,23]. The solution flux ($J_v$) can be determined by incorporating an additional term of cake resistance as follows:

$$J_v = \frac{(\Delta P - \sigma\Delta\pi)}{\mu\left(R_{m,s} + R_{non-rec} + R_c\right)} \quad (6)$$

where the subscript $s$ refers to salt; $R_{m,s} = (R_m + (1-\eta)R_{non-rec})/\eta$ is the membrane hydraulic resistance with the presence of salt ($m^{-1}$); $\eta$ is the permeability reduction factor (−) due to the effect of salt concentration at the membrane surface. The change in solution flux as a function of time can be written as follows [19]:

$$\frac{dJ_v}{dt} = -\frac{\sigma_s \alpha_s R_{mem,s}\beta_s}{\mu\left(R_{m,s} + R_{non-rec} + R_c\right)}\left(\frac{dC_{reten,s}}{dt}\right) - \frac{J_v}{\left(R_{m,s} + R_{non-rec} + R_c\right)}\left(\frac{dR_c}{dt}\right) \quad (7)$$

where $\alpha_s$ is the correlation between osmotic pressure and salt concentration (kPa L $mol^{-1}$); the ratio $\beta_s$ ($= C_{mem,s}/C_{reten,s}$) is the salt concentration polarization (−). $R_{mem,s}$ is the intrinsic membrane rejection in the presence of salt (−). $C_{mem,s}$ and $C_{reten,s}$ are salt concentration at the membrane surface and in the retentate (mol $L^{-1}$). The change in salt concentration in the retentate ($dC_{reten,s}/dt$) as a function of time can be determined based on the mass balance model using a completely stirred tank reactor [24].

### 2.4. Combined pore blockage, osmotic pressure and cake filtration model

Ho and Zydney [25] developed a model for dead-end filtration (microfiltration and ultrafiltration) of proteins that combines pore blockage and cake filtration mode of fouling. This model has been used to describe filtration of natural organic matter [9,21,26,27]. The model was further modified by incorporating a back transport term, modifying the model for application to crossflow systems [21]. Total flow through the membrane, ($Q_T = J_v A_m$), is the sum of the flow through open pores ($Q_{open} = J_{vo} A_{open}$) (L min$^{-1}$) (evaluated in terms of the clean membrane resistance) and through the presence of both blocked pores and cake formation ($Q_{blocked} = J_{blocked} A_{blocked}$) (L min$^{-1}$) [21].

$$\begin{aligned} Q_T &= J_v A_m = Q_{open} + Q_{blocked} \\ &= J_{vo} A_{open} + J_{blocked}\left(A_m - A_{open}\right) \end{aligned} \tag{8}$$

where $A_{open}$ is the area of the membrane, which remains unblocked (clean) (m$^2$); $A_{blocked}$ is the area of the membrane covered by cake deposition (m$^2$) ($A_{blocked} = A_m - A_{open}$); $J_{blocked}$ is the solution flux with cake formation on the membrane, which is described by additional term of cake resistance shown in Eq. (6). The rate of change in the number of pores (the rate of loss of open area) is assumed to be proportional to the net advective transport of solute to the membrane surface [21]:

$$\frac{dA_{open}}{dt} = -\alpha_{blocked} A_{open} C_{reten,NOM}(t)(J_{vo} - J^*). \tag{9}$$

Upon integration,

$$A_{open} = A_m \, exp\left(-\alpha_{blocked} C_{reten,NOM}(t)(J_{vo} - J^*)t\right). \tag{10}$$

In the classical cake filtration model, cake growth has been assumed to occur simultaneously with the pore coverage (or pore blockage) of the remaining open area of the membrane [19]. From Eq. (8), therefore, the change in solution flux as a function of time can be determined as follows:

$$\frac{dJ_v}{dt} = J_{vo}\frac{dA_{open}}{A_m dt} + J_{blocked}\frac{d\left(A_m - A_{open}\right)}{A_m dt} + \frac{\left(A_m - A_{open}\right)}{A_m}\frac{dJ_{blocked}}{dt}. \tag{11}$$

Eqs. (4) to (7) can be incorporated in the Eq. (11). Therefore, the change in solution flux during crossflow nanofiltration ($dJ_v/dt$) can be represented as follows:

$$\begin{aligned} \frac{dJ_v}{dt} = &-\left(1 - \frac{R_m}{R_{m,s} + R_{non-rec} + R_c}\right)\alpha_{blocked} C_{reten,NOM}(t) J_{vo}(J_{vo} - J^*) \\ &- \frac{\left(A_m - A_{open}\right)}{A_m}\left[\frac{\sigma_s \alpha_s R_{mem,s} \beta_s}{\mu\left(R_{m,s} + R_{non-rec} + R_c\right)}\left(\frac{dC_{reten,s}}{dt}\right)\right. \\ &\left. - \frac{J_v}{\left(R_{m,s} + R_{non-rec} + R_c\right)}\left(\frac{dR_c}{dt}\right)\right] \end{aligned} \tag{12}$$

The change in cake resistance ($dR_c/dt$) can be written as follows:

$$\frac{dR_c}{dt} = \alpha_{cake}\frac{dm_{cake}}{A_m dt} = \alpha_{cake} C_{reten,NOM}(t)(J_v - J^*) \tag{13}$$

where $m_{cake}$ is the cake mass (kg), $\alpha_{cake}$ is the specific cake resistance (m kg$^{-1}$). Eq. (12) is, therefore, a combined pore blockage, osmotic pressure and cake filtration model for crossflow nanofiltration. The model parameters of Eqs. (12) and (13) (i.e. $\alpha_{blocked}$, $\alpha_{cake}$, $J^*$, and $R_{m,s}$) can be estimated by non-linear curve fitting combined with a fourth-order Runge-Kutta routine for solving the differential equations. The sum squared errors (SSEs) between the experimental data and estimated data from the model can be determined in order to obtain the best fitting model parameters. The fitted model parameters were statistically determined based on 95% confidence interval for non-linear regression described by Draper and Smith [28]. For the experimental analysis, normalized solution flux with time can be determined by the ratio between solution flux and an initial flux solution. The combined pore blockage, osmotic pressure and cake filtration model (Eq. (12)) was used with the experimental results in order to evaluate model parameters of membrane fouling characteristics with different inorganic salts and ionic strength.

## 3. Experimental

### 3.1. Feed water

Feed water was obtained from the surface water reservoir at Ubon Ratchathani University (UBU), Thailand, which served as water supply for UBU community. The water characteristics were previously shown by Jarusutthirak et al. [12]. Natural organic matter (NOM) was isolated by using a polyamide thin-film composite (TFC) reverse osmosis (RO) membrane (model: AG4040F-spiral wound crossflow, GE osmonics, USA). The isolation procedure was previously described by Jarusutthirak et al. [12] and by Kilduff et al. [29]. The isolated NOM was diluted with deionized water. After dilution, the concentrations of NOM and NaCl (previously present in the feed water) were approximately 10 mg L$^{-1}$ and 0.7 meq L$^{-1}$, while the salt concentrations were adjusted to achieve the required ionic strengths (i.e. 0.01 M and 0.05 M) with different inorganic salts.

### 3.2. Inorganic salts

Inorganic salts applied in this study were sodium chloride (NaCl), calcium chloride ($CaCl_2$), calcium carbonate ($CaCO_3$), calcium phosphate ($Ca_3(PO_4)_2$), calcium sulphate dihydrate ($CaSO_4 \cdot 2H_2O$), and magnesium sulphate heptahydrate ($MgSO_4 \cdot 7H_2O$). Solutions containing inorganic salts were prepared to obtain ionic strengths (I.S.) of 0.01 M and 0.05 M. NOM concentrations of 10 mg L$^{-1}$ with solution pH of 7 were maintained constant throughout filtration experiments.

### 3.3. Crossflow nanofiltration test cell

Crossflow nanofiltration test cell with a recycle loop, previously described by Jarusutthirak et al. [12], was used to determine filtration performance during nanofiltration of NOM. This system consists of a stainless steel test cell (SEPA, Osmonics) that houses a single membrane sheet of 0.014 m$^2$ with a maximum operating pressure of 1000 psi. Thin-film nanofiltration membrane, obtained from GE Osmonics, Inc. USA, was used to investigate filtration characteristics during NF experiments. Membrane sheets were initially cleaned and pre-compacted with deionized water. After membrane compaction, average membrane permeability ($L_p$), of 16 samples, was $4.152 \times 10^{-8} \pm 0.062 \times 10^{-8}$ m s$^{-1}$ kPa$^{-1}$ (0.149 LMH kPa$^{-1}$ at 25 °C). The membrane hydraulic resistance ($R_m = 1/\mu L_p$), calculated with clean water as a function of operating pressures, was to be $2.694 \times 10^{13}$ m$^{-1}$. The membranes were stored in 1% $Na_2S_2O_5$ and kept in a refrigerator (4 °C) to minimize bacterial activity.

Solution flux was adjusted to achieve an initial solution flux of 45 LMH with a constant operating pressure during filtration. The membrane system was operated at recovery of 85% and crossflow velocity of 0.1 m s$^{-1}$. The filtration procedure and membrane cleaning were previously described by Jarusutthirak et al. [18]. Water flux recovery was determined for different inorganic salts after hydrodynamic and chemical cleaning.

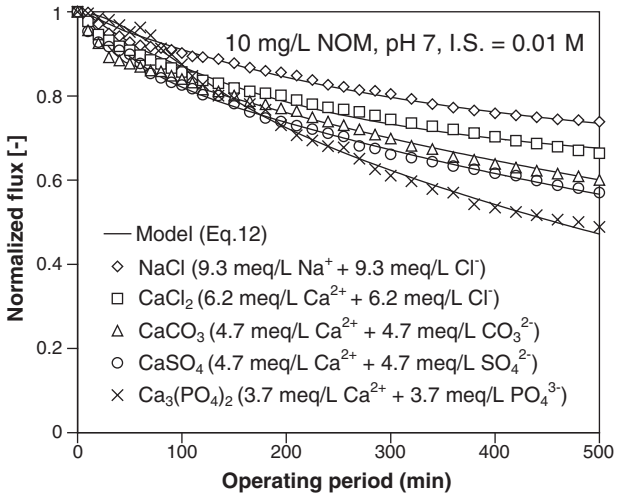


**Fig. 1.** Normalized flux for different inorganic salts (I.S. = 0.01 M).

### 3.4. Analytical methods

The concentrations of NOM were measured as dissolved organic matter using total organic carbon analyzer (Shimadzu Corporation, TOC-VCPH model, Japan). Potassium hydrogen phthalate (KHP) dissolved in deionized water was used as standard solution for adjusting TOC concentration. UV absorbance was determined at a wavelength of 254 nm using a UV–visible spectrophotometer (Shimadzu Corporation, model UV mini 1240, Japan). Conductivity and solution pH were examined using conductivity meter (model: inoLab cond Level 2, Germany) and pH meter (model: inoLab pH level 1, Wissenschaftlich-Technische Werkstatten, GMBH, Germany), respectively. The membrane surface characteristics before and after filtration experiments with different inorganic salts were examined by a scanning electron microscope (SEM, Leo Co., Ltd., model 1455 VP).

## 4. Results and discussion

### 4.1. Effect of different inorganic salts on normalized flux and model parameters

Fig. 1 exhibits the normalized flux for different inorganic salts with ionic strength of 0.01 M, while the model parameters are tabulated in Table 1. Dot points were the experimental data, while the solid lines were fitted relatively well with the modified mathematical fouling model (Eq. (12)). Each solution contained 10 mg $L^{-1}$ NOM and pH of 7 with NaCl concentration of 0.7 meq $L^{-1}$. From the figure, solution flux decline ranged in the order: $PO_4^{3-}$>$SO_4^{2-}$>$CO_3^{2-}$>$Cl^-$ species or normalized fluxes were 0.489, 0.57, 0.60, and 0.664 for phosphate, sulphate, carbonate, and chloride species, respectively. For chloride species, calcium ion with low feed concentration of 6.2 meq $L^{-1}$ presented greater flux decline than sodium ion with high feed concentration of 9.3 meq $L^{-1}$. The results suggested that divalent cation had significant effect on flux decline and rejection due to reduced charge repulsion between negatively charged NF membrane and positively charged cation. The results are attributed to a reduction of double layer thickness on the membrane surface and pores, thus increased membrane hydraulic resistance with the presence of salt ($R_{m,s}$) from $2.694\times10^{13}$ $m^{-1}$ to $3.63\times10^{13}$ $m^{-1}$ for NaCl and from $2.694\times10^{13}$ $m^{-1}$ to $4.13\times10^{13}$ $m^{-1}$ for $CaCl_2$. The salt rejections ($R_{reten,s}$) were relatively low about 24.4% for $CaCl_2$ to 25.3% for NaCl, indicating low salt rejecting NF membrane. Based on the model evaluation (Eq. (12)), the pore blockage efficiencies ($\alpha_{blocked}$) were relatively low for both sodium chloride and calcium chloride when compared with those of other inorganic salts (i.e. $CaCO_3$, $CaSO_4$, and $Ca_3(PO_4)_2$). The $\alpha_{blocked}$ parameters were about $6.07\pm1.77$, $9.13\pm2.43$, and $12.33\pm0.95$ $m^2kg^{-1}$ for inorganic salts containing carbonate, sulphate, and phosphate species, respectively. The results indicated that the pore blockage was less significant for chloride species during NF of NOM solution. The corresponding discussion related to solubility product constant ($K_{sp}$) is presented in last paragraph of this section. From Table 1, the specific cake resistances ($\alpha_{cake}$) were relatively high, indicating significant fouling potential caused by NOM cake formation at the membrane surface, especially for solution containing calcium chloride. Other inorganic salts (i.e. $CaCO_3$, $CaSO_4$, and $Ca_3(PO_4)_2$) with similar cation ion (i.e. $Ca^{2+}$) resulted in greater flux decline than calcium chloride and sodium chloride. The model parameters of $J^*$ tended to decrease, while the $R_{m,s}$ and $\alpha_{blocked}$ increased for $CO_3^{2-}$, $SO_4^{2-}$, and $PO_4^{3-}$ species. These values were significantly different from those of sodium chloride and calcium chloride. Calcium phosphate exhibited the greatest flux decline, supported by the increase of $R_{m,s}$ from $2.694\times10^{13}$ $m^{-1}$ to $13.01\times10^{13}$ $m^{-1}$. The increase in $R_{m,s}$ suggested that salt concentration at the membrane exceeded the solubility limit, thus enhancing a thicker precipitated salt formed at the membrane surface, while the pore blockage illustrated significant effects on membrane performance and fouling phenomena. For most inorganic salts, the averaged NOM rejections were relatively high (>93%). The averaged salt rejections ($R_{reten,s}$) of $CO_3^{2-}$, $SO_4^{2-}$, and $PO_4^{3-}$ species were higher than those of $Cl^-$, possibly due to higher charge repulsion in order to maintain electroneutrality condition leading to high salt rejection.

Fig. 2 presents the normalized flux for different inorganic salts with ionic strength of 0.05 M, while the model parameters are tabulated in Table 2. The experimental results exhibited similar trend with low ionic strength of 0.01 M (Fig. 1 and Table 1). From the figure, the normalized fluxes were fitted relatively well between the experimental data and the modified mathematical fouling model. The flux declines ranged in the order: $Ca_3(PO_4)_2$>$CaSO_4$>$CaCO_3$>$CaCl_2$>NaCl. The normalized fluxes were 0.278($Ca_3(PO_4)_2$), 0.561($CaSO_4$), 0.584($CaCO_3$), 0.648 ($CaCl_2$), and 0.723(NaCl), indicating an increase in flux decline with increasing ionic strength. Increased ionic strengths resulted in an increased $R_{m,s}$ for $2.694\times10^{13}$ $m^{-1}$ to $4.13\times10^{13}$ $m^{-1}$ for NaCl and from $2.694\times10^{13}$ $m^{-1}$ to $4.81\times10^{13}$ $m^{-1}$ for $CaCl_2$. For NaCl and $CaCl_2$

**Table 1**
Membrane performance and model parameters for inorganic salts (I.S. = 0.01 M).

| Parameters | Inorganic salts | | | | |
|---|---|---|---|---|---|
| | NaCl | $CaCl_2$ | $CaCO_3$ | $CaSO_4$ | $Ca_3(PO_4)_2$ |
| $J_v/J_{vo}$ (−) | 0.739 | 0.664 | 0.60 | 0.57 | 0.489 |
| $J^*$ ($m\,s^{-1}$)$\times10^6$ | $10.08\pm0.15$ | $9.54\pm0.16$ | $7.51\pm0.31$ | $7.09\pm0.38$ | $5.92\pm0.22$ |
| $R_{reten,s}$ (%) | $25.3\pm0.6$ | $24.2\pm0.9$ | $54.2\pm2.8$ | $72.7\pm2.7$ | $65.8\pm10.1$ |
| $R_{reten,NOM}$ (%) | $94.9\pm1.1$ | $97.0\pm0.9$ | $96.5\pm0.8$ | $93.3\pm2.0$ | $93.0\pm1.5$ |
| $R_{m,s}$ ($m^{-1}$)$\times10^{-13}$ | $3.63\pm0.21$ | $4.13\pm0.33$ | $9.31\pm0.28$ | $11.67\pm0.33$ | $13.01\pm0.51$ |
| $\alpha_{blocked}$ ($m^2kg^{-1}$) | 0.75 | 0.67 | $6.07\pm1.77$ | $9.13\pm2.43$ | $12.33\pm0.95$ |
| $\alpha_{cake}$ ($m.kg^{-1}$)$\times10^{-15}$ | $3.73\pm0.99$ | $6.0\pm2.45$ | $2.64\pm0.62$ | $4.02\pm0.94$ | $3.37\pm0.43$ |

The membrane hydraulic resistance ($R_m$) was about $2.694\times10^{13}$ $m^{-1}$. The $R_{reten,s}$ and $R_{reten,NOM}$ are the salt rejection and NOM rejection in the retentate. The values were determined within the 95% confidence interval for the model parameters.

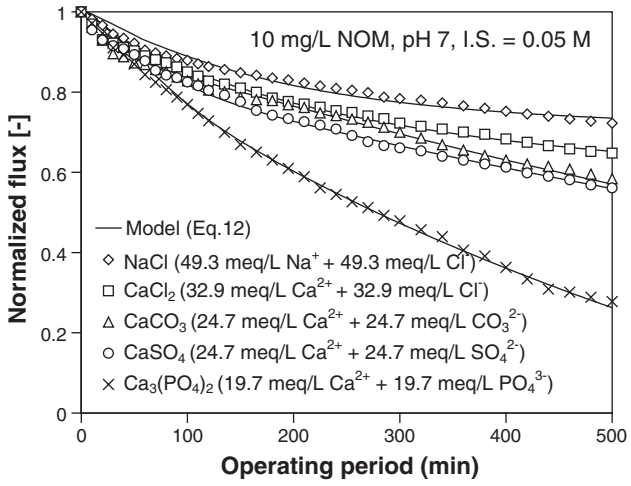


**Fig. 2.** Normalized flux for different inorganic salts (I.S. = 0.05 M).

species, the increase in $R_{m,s}$ and $\alpha_{cake}$ showed significant effects from osmotic pressure caused by salt concentration and NOM cake formation, respectively. For $CO_3^{2-}$, $SO_4^{2-}$, and $PO_4^{3-}$ species, the precipitated salts could possibly cause significant effects in $R_{m,s}$ and $\alpha_{blocked}$. It was evident that phosphate species showed the highest flux decline and $\alpha_{blocked}$. This suggested that precipitated-phosphate salt affected nanofiltration performance parameters.

Fig. 3 depicts the membrane SEM images for different inorganic salts (10 mg $L^{-1}$ NOM and I.S. = 0.05 M). The membrane surface images for solutions containing NaCl and $CaCl_2$ exhibited NOM cake formation on the membrane surface, when compared with the "clean" membrane surface shown in Fig. 3(a). Solutions having $CO_3^{2-}$, $SO_4^{2-}$, and $PO_4^{3-}$ species exhibited precipitated salts at the membrane surface. The morphological characteristics of the precipitated salts for $CO_3^{2-}$, $SO_4^{2-}$, and $PO_4^{3-}$ species were quite different than those for NaCl and $CaCl_2$ (NOM cake formation). The precipitated layer appears to be somewhat denser and thicker than the cake layer of NaCl and $CaCl_2$ solution.

Fig. 4 expresses the pore blockage efficiency ($\alpha_{blocked}$) for inorganic salts with different ionic strengths. With increasing ionic strength from 0.01 M to 0.05 M, the $\alpha_{blocked}$ values increased for most inorganic salts, while the $\alpha_{blocked}$ values were relatively low and not significantly different for NaCl and $CaCl_2$ solution. This indicated that the pore blockage values of chloride species (i.e. NaCl and $CaCl_2$) were less than those of carbonate, sulphate, and phosphate species. At ionic strength of 0.05 M, the values of $\alpha_{blocked}$ for $CO_3^{2-}$, $SO_4^{2-}$, and $PO_4^{3-}$ species were approximately $6.50 \pm 0.77$, $10.25 \pm 2.18$, and $12.59 \pm 0.59$ $m^2\,kg^{-1}$, respectively. This suggested that the precipitated salts could possibly block pore entrances due to increased salt concentration during filtration.

Fig. 5 exhibits the membrane hydraulic resistance with the presence of salt ($R_{m,s}$) for inorganic salts with different ionic strengths. The $R_{m,s}$ values of chloride species (i.e. NaCl and $CaCl_2$) were relatively low and slightly increased with increasing ionic strengths. This was possibly caused by reduced charge repulsion between positively charged cation ion and negatively charged NF membrane, thus compressing a double layer thickness at the membrane surface [19]. The presence of salt could reduce membrane permeability (i.e. increased $R_{m,s}$). The increase in $R_{m,s}$ was found to be significant with increasing ionic strengths for carbonate, sulphate, and phosphate species. With increasing ionic strength, the increase in $R_{m,s}$ for carbonate, sulphate, and phosphate species was possibly due to increased salt concentration on the membrane surface, thus exceeding solubility product constant ($K_{sp}$) (precipitated salts occurred). The $K_{sp}$ values for carbonate, sulphate, and phosphate species were about $10^{-8.34}$, $10^{-4.7}$, and $10^{-54.1}$, respectively [30].

### 4.2. Effect of ionic strengths on normalized flux and model parameters for $Ca_3(PO_4)_2$

Fig. 6 illustrates the effect of ionic strength on normalized flux for $Ca_3(PO_4)_2$, while the model parameters are tabulated in Table 3. Phosphate species was selected to examine the effect of ionic strengths on normalized flux and model parameters because the phosphate species ($Ca_3(PO_4)_2$) exhibited the greatest flux decline when compared with other inorganic salts. From the figure, the experimental data were fitted relatively well with the combined mathematical fouling model (Eq. (12)). Increased ionic strengths increased normalized flux decline, while the flux decline was significantly pronounced at the highest ionic strength (0.11 M). Normalized flux decreased from 0.489 to 0.135 with increasing ionic strength from 0.01 M (3.7 meq $L^{-1}$ $Ca_3(PO_4)_2$ to 0.11 M (19.7 meq $L^{-1}$ $Ca_3(PO_4)_2$). The results exhibited an increased $R_{m,s}$ ranging from $13.01 \times 10^{13}$ $m^{-1}$ to $40.48 \times 10^{13}$ $m^{-1}$. This was possibly caused by precipitated salt at the membrane surface and/or pores due to relatively low solubility product constants ($K_{sp}$) of phosphate species (i.e. $CaHPO_{4(s)}$ ($K_{sp} = 10^{-6.52}$), $Ca_5(PO_4)_3OH_{(s)}$ ($K_{sp} = 10^{-54.1}$), and $Ca_3(PO_4)_{2(s)}$ ($K_{sp} = 10^{-27}$)[30]). The results corresponded to increase $\alpha_{blocked}$ and $\alpha_{cake}$ with increasing ionic strengths as shown in Fig. 7. The $\alpha_{blocked}$ and $\alpha_{cake}$ values ranged from $11.83 \pm 0.83$ to $24.94 \pm 1.58$ $m^2 kg^{-1}$ and $2.38 \pm 0.79 \times 10^{15}$ to $38.72 \pm 0.46 \times 10^{15}$ $m\,kg^{-1}$, respectively. The model parameters were found to be significant at the highest ionic strength of 0.11 M. Increased ionic strengths tended to increase averaged salt rejections ranging from 65.8% to 69.2%, while NOM rejections were relatively high from 92.1% to 95.9%. Previous study indicated that the increase in ionic strength (i.e. NaCl) decreased the salt rejection, while the salt rejections increased with increasing ionic strengths using calcium chloride, indicating calcium–NOM accumulation on the membrane surface [19]. The experimental results could confirm the combination of fouling mechanisms due to membrane surface blockage and/or pore blockage from precipitated salt, osmotic pressure caused by increased salt concentration, and cake formation based on NOM cake formation, which significantly influenced nanofiltration performance and model parameters.

**Table 2**
Membrane performance and model parameters for inorganic salts (I.S. = 0.05 M).

| Parameters | Inorganic salts | | | | |
|---|---|---|---|---|---|
| | NaCl | $CaCl_2$ | $CaCO_3$ | $CaSO_4$ | $Ca_3(PO_4)_2$ |
| $J_v/J_{vo}$ (−) | 0.723 | 0.648 | 0.584 | 0.561 | 0.278 |
| $J^*$ ($m\,s^{-1}$) $\times 10^6$ | $10.03 \pm 0.14$ | $9.05 \pm 0.14$ | $7.33 \pm 0.31$ | $6.92 \pm 0.78$ | $3.87 \pm 0.29$ |
| $R_{reten,s}$ (%) | $13.7 \pm 2.5$ | $38.2 \pm 0.2$ | $48.6 \pm 6.3$ | $80.2 \pm 2.0$ | $68.3 \pm 3.9$ |
| $R_{reten,NOM}$ (%) | $95.3 \pm 1.4$ | $95.7 \pm 1.1$ | $97.4 \pm 1.0$ | $93.1 \pm 0.7$ | $92.1 \pm 1.8$ |
| $R_{m,s}$ ($m^{-1}$) $\times 10^{-13}$ | $4.13 \pm 0.39$ | $4.81 \pm 0.27$ | $34.47 \pm 1.16$ | $49.61 \pm 1.39$ | $35.44 \pm 0.89$ |
| $\alpha_{blocked}$ ($m^2 kg^{-1}$) | 0.79 | 0.64 | $6.50 \pm 0.77$ | $10.25 \pm 2.18$ | $12.59 \pm 0.59$ |
| $\alpha_{cake}$ ($m.kg^{-1}$) $\times 10^{-15}$ | $7.98 \pm 3.25$ | $8.22 \pm 2.15$ | $3.24 \pm 1.42$ | $3.91 \pm 3.27$ | $3.54 \pm 1.30$ |

The membrane hydraulic resistance ($R_m$) was about $2.694 \times 10^{13}$ $m^{-1}$. The $R_{reten,s}$ and $R_{reten,NOM}$ are the salt rejection and NOM rejection in the retentate. The values were determined within the 95% confidence interval for the model parameters.

*4.3. Effect of different divalent inorganic salts on normalized flux and model parameters*

Fig. 8 describes the effect of divalent inorganic salt on normalized flux. Solutions contained 4.7 meq $L^{-1}$ and 24.7 meq $L^{-1}$ divalent inorganic salts ($Ca^{2+}$ and $Mg^{2+}$) for low (0.01 M) and high ionic strength (0.05 M), respectively. Solutions having divalent calcium resulted in greater flux decline than those having divalent magnesium. Increased ionic strengths did not give significant difference in flux decline for both $CaSO_4$ and $MgSO_4$ salts. With increasing ionic strengths, the salt rejections in the retentate ($R_{reten,s}$) slightly increased from 72.7% to 80.2% for $CaSO_4$ and from 75.9% to 80.2% for $MgSO_4$. The averaged rejections of $Ca^{2+}$ and $SO_4^{2-}$ species were relatively high about 83.6% and 83.7%, respectively. The averaged rejections of $Mg^{2+}$ and $SO_4^{2-}$ ions were relatively high about 85.2% and 85.7%, indicating greater ion rejections than divalent calcium. The experimental results indicated a charge balance (electroneutrality) for positive and negative ions in the retentate, while increased ionic strengths resulted in a slight increase of ion rejections for both $CaSO_4$ and $MgSO_4$ salts. The results suggested a decrease in charge repulsion at the membrane surface, thus indicating compressed double layer thickness at the membrane [31].

For both divalent inorganic salts, the averaged rejections of NOM were relatively high in the range from 93.1% to 95.3%. Based on the modified mathematical fouling model (Eq. (12)), flux declines were possibly caused by precipitated salts at the membrane surface and/or pores, thus increased $\alpha_{blocked}$ *and* $R_{m,s}$. The model parameters (i.e.$\alpha_{blocked}$ *and* $R_{m,s}$) increased for both divalent inorganic salts as ionic strengths increased. Fig. 9 depicts the membrane SEM images for $CaSO_4$ and $MgSO_4$ salts (10 mg $L^{-1}$ NOM, I.S. = 0.05 M). This

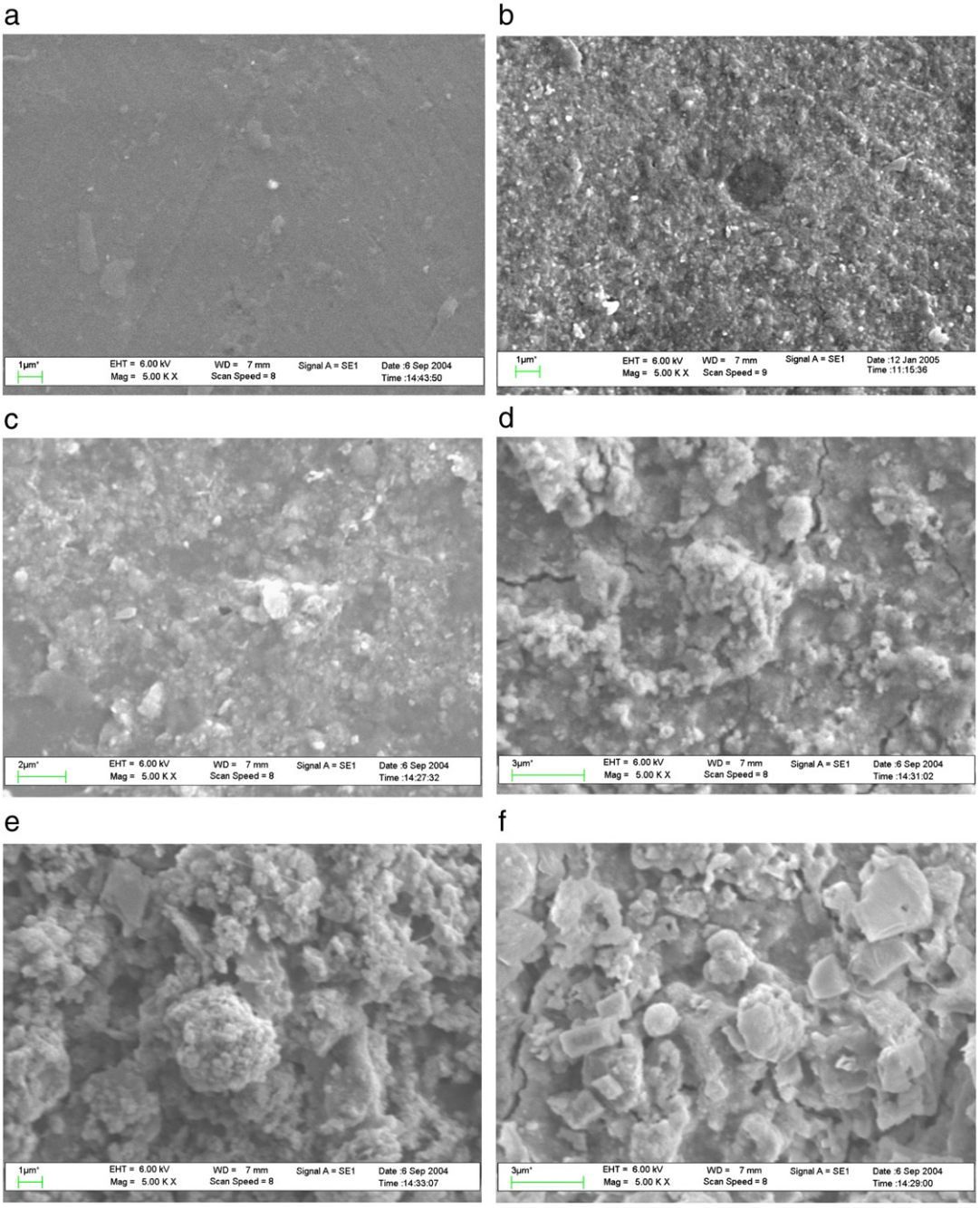


**Fig. 3.** Scanning electron microscopy (SEM) images of different inorganic salts. (10 mg $L^{-1}$ NOM, I.S. = 0.05 M) (a) New membrane (b) NaCl (c) $CaCl_2$ (d) $CaCO_3$ (e) $CaSO_4$ and (f) $Ca_3(PO_4)_2$.

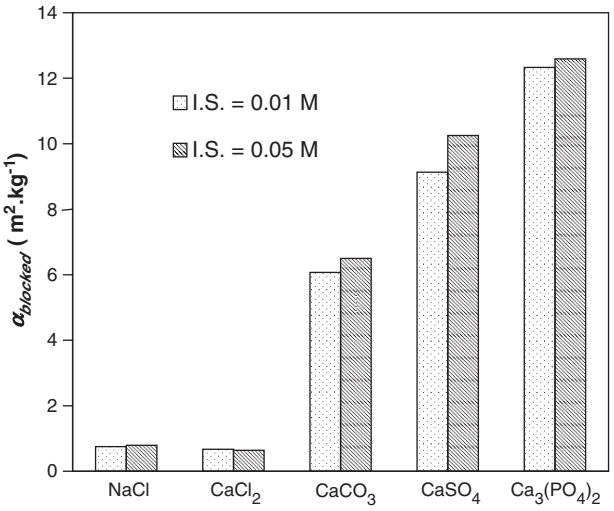


**Fig. 4.** Pore blockage efficiency ($\alpha_{blocked}$) for inorganic salts with different ionic strengths.

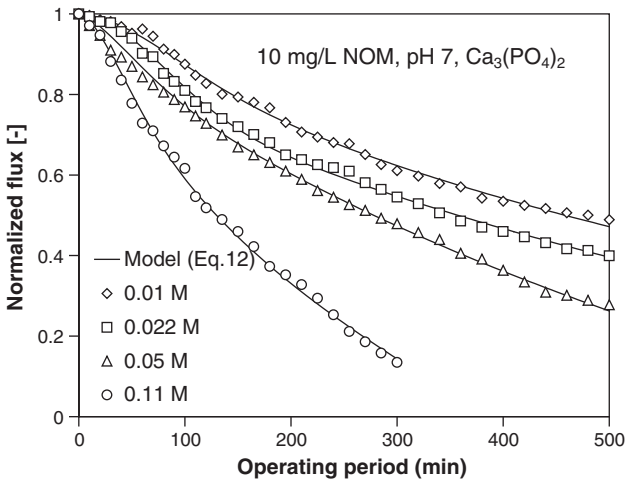


**Fig. 6.** Effect of ionic strength on normalized flux for $Ca_3(PO_4)_2$.

figure indicated that calcium sulphate could form precipitated salt (i.e. $CaSO_{4(s)}$ with solubility product constant of $10^{-4.7}$[30]). The increase in salt concentrations was pronounced during filtration experiment, thus inducing precipitated salt at the membrane surface. Magnesium sulphate could cause precipitated salt with relatively high salt rejections and NOM rejections compared with calcium sulphate. The solubility product constants for $Mg(OH)_{2(s)}$ and $MgSO_4 \cdot 7H_2O_{(s)}$ were about $10^{-11.05}$ [30] and about $10^{-2.14}$ based on MINEQL+program for chemical equilibrium system, respectively. Precipitated species for $MgSO_4 \cdot 7H_2O_{(s)}$ could possibly form during filtration due to increased salt concentrations (i.e. $Mg^{2+}$ and $SO_4^{2-}$ ion) throughout filtration, while the precipitated salt of $Mg(OH)_{2(s)}$ was least possible for salt precipitation due to low concentration of proton ($[H^+] = 10^{-7}$M, solution pH of 7). Solution flux of precipitated divalent calcium exhibited greater flux decline than divalent magnesium. This was possibly caused by precipitated salt, which attributed to increased osmotic pressure based on salt concentration polarization and hydraulic resistance effects from precipitated salt.

### 4.4. Effect of different inorganic salts on water flux recovery and salt rejections

Fig. 10 shows water flux recovery for inorganic salts with different ionic strengths. Water flux recovery was determined after hydrodynamic and chemical cleaning. For monovalent cation ($Na^+$), water flux recoveries after hydrodynamic and chemical cleaning were relatively high about 0.938 and 0.964 (at ionic strength of 0.01 M) and low about 0.894 and 0.937 (at ionic strength of 0.05 M), respectively. The experimental results demonstrated reversible fouling caused by compacted salt-NOM cake layer. After chemical cleaning, water flux recovery of divalent cation ($Ca^{2+}$) was lower than that of monovalent cation ($Na^+$) about 0.862 (at ionic strength of 0.01 M) and 0.848 (at ionic strength of 0.05 M), suggesting a more compacted Ca-NOM cake layer, thus increased $\alpha_{cake}$ and non-recoverable resistances ($R_{non\text{-}rec}$). For different salt species, water flux recovery seemed to follow the same order as solution flux curve (i.e. $Cl^-$, $CO_3^{2-}$, $SO_4^{2-}$, and $PO_4^{3-}$). The water flux recoveries of precipitated species (i.e. $CO_3^{2-}$, $SO_4^{2-}$, and $PO_4^{3-}$) were relatively low, especially for $PO_4^{3-}$ species. At ionic strength of 0.05 M, the water flux recoveries for phosphate species were relatively low about 0.33 (−) for hydrodynamic cleaning and 0.58 (−) for chemical cleaning. The experimental results could partly be explained by increased non-recoverable resistance ($R_{non\text{-}rec}$) due to pore plugging of precipitated salts in and within the membrane pore matrix. Solutions containing divalent calcium exhibited lower water flux recovery than those containing divalent magnesium, corresponding to greater flux decline caused by calcium salt precipitation.

Fig. 11 illustrates the conductivity rejections for different inorganic salts. The conductivity rejections were relatively low for solutions containing NaCl (25.3 ± 0.6%) and $CaCl_2$ (24.2 ± 0.9%), while the conductivity rejections ranged in the order: $MgSO_4$>$CaSO_4$>$Ca_3(PO_4)_2$>$CaCO_3$. As previously reported [32], the conductivity rejections of $MgSO_4$ exhibited greater values than those of $CaCl_2$, because a negatively charged $SO_4^{2-}$ species had higher charge density, which

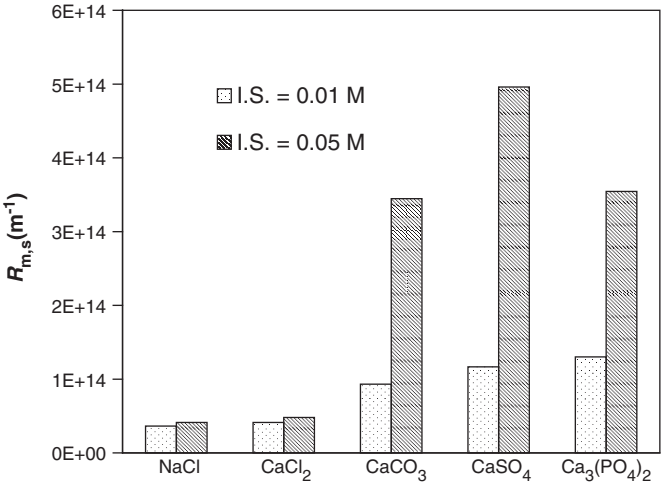


**Fig. 5.** Membrane hydraulic resistance with the presence of salt ($R_{m,s}$) for inorganic salts with different ionic strengths.

**Table 3**
Effect of ionic strengths on membrane performance and model parameters for $Ca_3(PO_4)_2$.

| Parameters | Ionic strength (M) | | | |
|---|---|---|---|---|
| | 0.01 | 0.022 | 0.05 | 0.11 |
| $J_v/J_{vo}$ (−) | 0.489 | 0.399 | 0.278 | 0.135 |
| $J^*$ (m s$^{-1}$)×10$^6$ | 5.92 ± 0.22 | 5.31 ± 0.28 | 3.87 ± 0.29 | 1.71 ± 0.30 |
| $R_{reten,s}$ (%) | 65.8 ± 10.1 | 66.8 ± 11.3 | 68.3 ± 3.9 | 69.1 ± 5.5 |
| $R_{reten,NOM}$ (%) | 93.0 ± 1.5 | 95.9 ± 3.7 | 92.1 ± 1.8 | 95.6 ± 1.1 |
| $R_{m,s}$ (m$^{-1}$)×10$^{-13}$ | 13.01 ± 0.51 | 14.18 ± 0.29 | 35.44 ± 0.89 | 40.48 ± 1.19 |
| $\alpha_{blocked}$ (m$^2$kg$^{-1}$) | 12.33 ± 0.95 | 11.83 ± 0.83 | 12.59 ± 0.59 | 24.94 ± 1.58 |
| $\alpha_{cake}$ (m.kg$^{-1}$)×10$^{-15}$ | 3.37 ± 0.43 | 2.38 ± 0.79 | 3.54 ± 1.30 | 38.72 ± 0.46 |

The membrane hydraulic resistance ($R_m$) was about 2.694×10$^{13}$ m$^{-1}$. The $R_{reten,s}$ and $R_{reten,NOM}$ are the salt rejection and NOM rejection in the retentate. The values were determined within the 95% confidence interval for the model parameters.

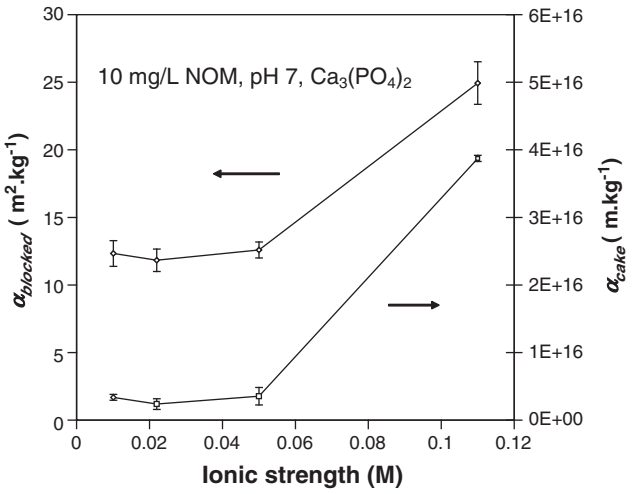


**Fig. 7.** Effect of ionic strength on $\alpha_{blocked}$ and $\alpha_{cake}$ for $Ca_3(PO_4)_2$.

was possibly rejected by the negatively charged NF membrane. The negatively charged anions were rejected from the negatively charged NF membrane, causing the rejection of the positively charged cations in order to keep electroneutrality condition. The results enhanced salt precipitation fouling beyond their solubility limits. Salt precipitation was possibly occurred due to increased salt concentration during permeate withdrawal, which was further enhanced in the region next to the membrane surface by the superimposed effect of concentration polarization [15].

## 5. Conclusions

A combined mathematical fouling model based on pore blockage, osmotic pressure, and cake filtration model can be successfully used to determine nanofiltration performance and model parameters (i.e. $\alpha_{blocked}$, $\alpha_{cake}$, $J^*$ , and $R_{m,s}$) for crossflow nanofiltration of NOM solution and inorganic salts. The pore blockage efficiencies ($\alpha_{blocked}$) for the pore blockage model were determined for membrane pore blocking effects, while the specific cake resistances ($\alpha_{cake}$) were used to explain the cake formation due to NOM accumulation on the membrane surface. The salt concentrations enhanced an increase in osmotic pressure during NF experiments, thus increasing membrane hydraulic resistances with the presence of inorganic salts ($R_{m,s}$) for soluble inorganic salts (i.e. NaCl and $CaCl_2$), while increased salt concentration exceeded their solubility equilibrium for sparingly soluble inorganic salts (i.e. $CaCO_3$, $CaSO_4$, and $Ca_3(PO_4)_2$). The experimental results confirmed the appearance of precipitated salt, affecting an increase in $R_{m,s}$. For sparingly soluble inorganic salts, the model parameters (i.e.$\alpha_{blocked}$ and $R_{m,s}$) exhibited higher values than those for soluble inorganic salts, while the model parameter (i.e. $R_{m,s}$ and $\alpha_{cake}$) was found to be significant for soluble inorganic salts due to increased salt concentration and NOM cake accumulation at the membrane surface. Increased ionic strengths tended to increase the values of most model parameters for all inorganic salts. The $R_{m,s}$

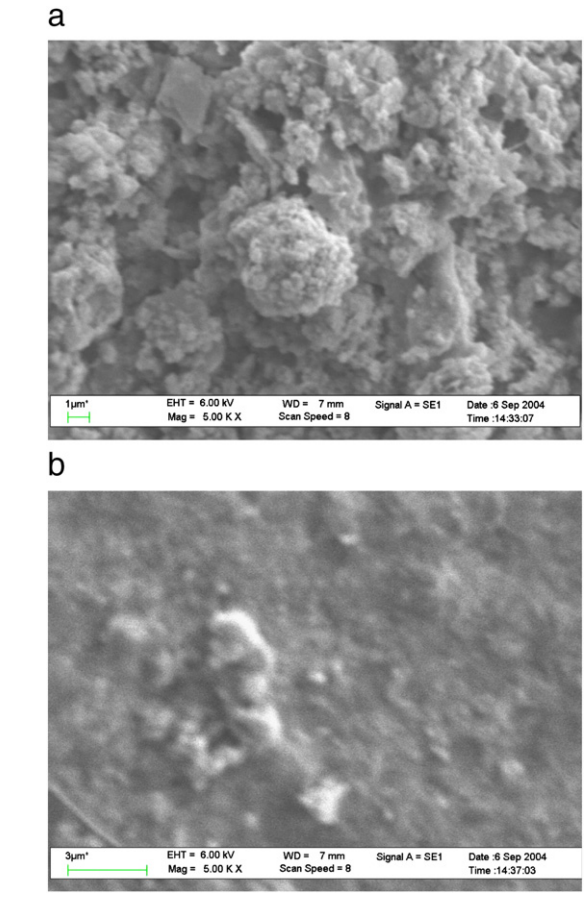


**Fig. 9.** Membrane SEM images (10 mg $L^{-1}$, I.S. = 0.05 M) (a) $CaSO_4$ and (b) $MgSO_4$.

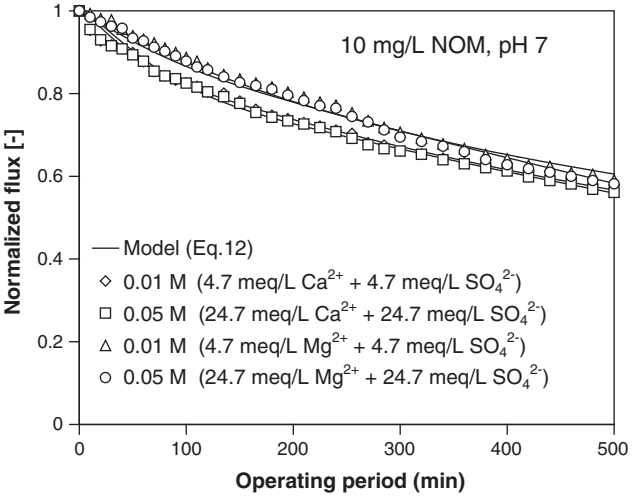


**Fig. 8.** Effect of divalent inorganic salt on normalized flux.

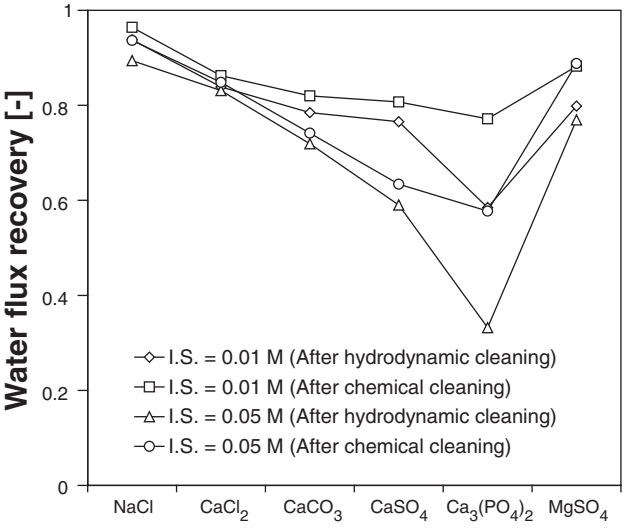


**Fig. 10.** Water flux recovery for inorganic salts with different ionic strengths.

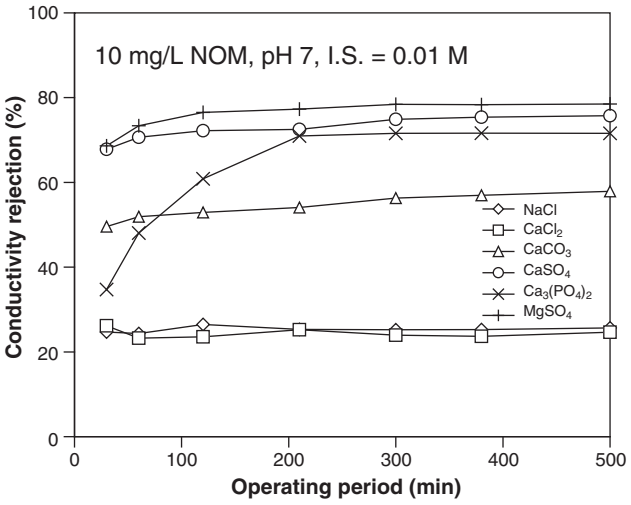


**Fig. 11.** Conductivity rejections for different inorganic salts.

increased significantly for sparingly soluble inorganic salts due to precipitated salt, thus increased $\alpha_{blocked}$ values. The reduction in flux decline was the most pronounced for phosphate species, suggesting the combination effects in membrane pore blockage, increased osmotic pressure from salt concentration polarization during filtration, and cake formation at the membrane surface. Membrane surfaces were examined by SEM to elucidate the morphological characteristics of the precipitated salts. With different cations, the divalent calcium presented greater flux decline than divalent magnesium and monovalent sodium. Higher negatively charged anions (i.e. $CO_3^{2-}$, $SO_4^{2-}$, and $PO_4^{3-}$ species) illustrated greater charge repulsion than the lower negatively charged anion (i.e. $Cl^-$), thus leading to high salt rejection in order to maintain electroneutrality condition and salt precipitation effects at the membrane surface. The lowest water flux recovery for phosphate species indicated an increased non-recoverable resistance ($R_{non\text{-}rec}$) due to pore plugging of precipitated salt.

*Nomenclature*

| | |
|---|---|
| $A_{blocked}$ | area of the membrane covered by cake deposition ($m^2$) |
| $A_m$ | total active permeable membrane area ($m^2$) |
| $A_{open}$ | area of the membrane, which remains unblocked (clean) ($m^2$) |
| $A_{p,T}$ | total pore area ($m^2$) |
| $C_{mem}$ | solute concentration at the membrane surface (mol $L^{-1}$) |
| $C_{perm}$ | solute concentration in the permeate (mol $L^{-1}$) |
| $C_{mem,s}$ | salt concentration at the membrane surface (mol $L^{-1}$) |
| $C_{reten,NOM}$ | NOM concentration in the retentate (kg $m^{-3}$) |
| $C_{reten,s}$ | salt concentration in the retentate (mol $L^{-1}$) |
| $J_{blocked}$ | solution flux with cake formation on the membrane (L $m^{-2}h^{-1}$, LMH) |
| $J_v$ | solution flux (L $m^{-2}h^{-1}$, LMH) |
| $J_{vo}$ | clean water flux (L $m^{-2}h^{-1}$, LMH) |
| $J^*$ | effective flux associated with back-transport resulting from crossflow (LMH) |
| $K_{sp}$ | solubility product constant |
| $L_p$ | membrane permeability (LMH $kPa^{-1}$) |
| $m_{cake}$ | cake mass (kg) |
| $N$ | number of pores per unit membrane area (pores $m^{-2}$) |
| $\Delta P$ | transmembrane pressure (kPa) |
| $Q_{blocked}$ | flow through the presence of both blocked pores and cake formation (L $min^{-1}$) |
| $Q_{open}$ | flow through open pores (L $min^{-1}$) |
| $Q_T$ | total flow through the membrane (L $min^{-1}$) |
| $R_c$ | cake resistance ($m^{-1}$) |
| $R_m$ | membrane hydraulic resistance ($m^{-1}$) |
| $R_{mem}$ | intrinsic membrane rejection (−) |
| $R_{mem,s}$ | intrinsic membrane rejection in the presence of salt (−) |
| $R_{m,s}$ | membrane hydraulic resistance with the presence of salt ($m^{-1}$) |
| $R_{non\text{-}rec}$ | non-recoverable resistance ($m^{-1}$) |
| $R_{reten,s}$ | salt rejection in the retentate (−) |
| $R_{reten,NOM}$ | NOM rejection in the retentate (−) |
| $r_p$ | uniform membrane pore radius (m) |
| $t$ | operating period (min) |

*Greek Letters*

| | |
|---|---|
| $\alpha_{blocked}$ | pore blockage efficiency ($m^2 kg^{-1}$) |
| $\alpha_{cake}$ | specific cake resistance (m $kg^{-1}$) |
| $\alpha_s$ | correlation between osmotic pressure and salt concentration (kPa L $mol^{-1}$) |
| $\eta$ | permeability reduction factor (−) |
| $\beta_s$ | salt concentration polarization (−) |
| $\delta_m$ | membrane thickness (m) |
| $\mu$ | dynamic viscosity (kg $m^{-1}s^{-1}$) |
| $\pi$ | osmotic pressure (kPa) |
| $\pi_{mem}$ | osmotic pressure at the membrane surface (kPa) |
| $\pi_{perm}$ | osmotic pressure in the permeate (kPa) |
| $\sigma$ | osmotic reflection coefficient (−) |

## Acknowledgements

The authors would like to thank the Thailand Research Fund (TRF) for TRF senior research scholar grant (No. RTA5380001) for financial support. We also would like to acknowledge the Department of Chemical Engineering, Faculty of Engineering, Ubon Rachathani University, and the National Center of Excellence for Environmental and Hazardous Waste Management, Ubon Ratchathani University, Ubonratchathani, Thailand, for all experimental equipments applied in this research.

## References

[1] J.G. Jacangelo, R.R. Trussell, M. Watson, Role of membrane technology in drinking water treatment in the United States, Desalination 113 (1997) 119–127.
[2] A. de la Rubia, M. Rodriguez, V.M. Leon, D. Prats, Removal of natural organic matter and THM formation potential by ultra- and nanofiltration of surface, Water Res. 42 (2008) 714–722.
[3] A.W. Zularisam, A.F. Ismail, R. Salim, Behaviours of natural organic matter in membrane filtration for surface water treatment — a review, Desalination 194 (2006) 211–231.
[4] G. Belfort, R.H. Davis, A.L. Zydney, The behavior of suspensions and macromolecular solutions in cross-flow microfiltration, J. Membr. Sci. 96 (1994) 1–58.
[5] S. Shirazi, C.-H. Lin, D. Chen, Inorganic fouling of pressure-driven membrane processes — a critical review, Desalination 250 (2010) 236–248.
[6] N. Her, G. Amy, A. Plottu-Pecheux, Y. Yoon, Identification of nanofiltration membrane foulants, Water Res. 41 (2007) 3936–3947.
[7] E. Tipping, Cation binding by humic substances, Cambridge Environmental Chemistry Series, 1948, ISBN 0 521 62146 1.
[8] E.M. Thurman, Organic Geochemistry of Natural Waters, Martinus Nijhoff/Dr W. Junk Publishers, Dordrecht, 1985.
[9] M. Taniguchi, J.E. Kilduff, G. Belfort, Modes of natural organic matter fouling during ultrafiltration, Environ. Sci. Technol. 37 (2003) 1676–1683.
[10] W. Yuan, A.L. Zydney, Humic acid fouling during ultrafiltration, Environ. Sci. Technol. 34 (2000) 5043–5050.
[11] C.-F. Lin, A.Y.-C. Lin, P.S. Chandana, C.-Y. Tsai, Effects of mass retention of dissolved organic matter and membrane pore size on membrane fouling and flux decline, Water Res. 43 (2009) 389–394.
[12] C. Jarusutthirak, S. Mattaraj, R. Jiraratananon, Factors affecting nanofiltration performances in natural organic matter rejection and flux decline, Sep. Pur. Technol. 58 (2007) 68–75.
[13] C.-J. Lin, S. Shirazi, P. Rao, S. Agarwal, Effects of operational parameters on cake formation of $CaSO_4$ in nanofiltration, Water Res. 40 (2006) 806–816.
[14] S. Lee, J. Kim, C.-H. Lee, Analysis of $CaSO_4$ scale formation mechanism in various nanofiltration modules, J. Membr. Sci. 163 (1999) 63–74.

[15] Ch. Tzotzi, T. Pahiadaki, S.G. Yiantsios, A.J. Karabelas, N. Andritsos, A study of $CaCO_3$ scale formation and inhibition in RO and NF membrane processes, J. Membr. Sci. 296 (2007) 171–184.
[16] W. Saikaew, S. Mattaraj, R. Jiraratananon, Nanofiltration performance of lead solutions: effects of solution pH and ionic strength, Water Sci. Technol.: Water Supply 10 (2) (2010) 193–200.
[17] S. Hong, M. Elimelech, Chemical and physical aspects of natural organic matter (NOM) fouling of nanofiltration membranes, J. Membr. Sci. 132 (1997) 159–181.
[18] C. Jarusutthirak, S. Mattaraj, R. Jiraratananon, Influence of inorganic scalants and natural organic matter on nanofiltration membrane fouling, J. Membr. Sci. 287 (2007) 138–145.
[19] S. Mattaraj, C. Jarusutthirak, R. Jiraratananon, A combined osmotic pressure and cake filtration model for crossflow nanofiltration of natural organic matter, J. Membr. Sci. 322 (2008) 475–483.
[20] S. Mattaraj, W. Phimpha, P. Hongthong, R. Jiraratananon, Effect of operating conditions and solution chemistry on model parameters in crossflow reverse osmosis of natural organic matter, Desalination 253 (2010) 38–45.
[21] J.E. Kilduff, S. Mattaraj, J. Sensibaugh, J.P. Pieracci, Y. Yuan, G. Belfort, Modeling flux decline during nanofiltration of NOM with poly (arylsulfone) nanofiltration membranes modified using UV-Assisted graft polymerization, Environ. Eng. Sci. 19 (6) (2002) 477–496.
[22] R.W. Field, D. Wu, J.A. Howell, B.B. Gupta, Critical flux concept for microfiltration fouling, J. Membr. Sci. 100 (1995) 259–272.
[23] L.J. Zeman, A.L. Zydney, Microfiltration and ultrafiltration: Principles and Applications, M. Dekker, New York, 1996.
[24] J.E. Kilduff, S. Mattaraj, G. Belfort, Flux decline during nanofiltration of naturally-occurring dissolved organic matter: effects of osmotic pressure, membrane permeability, and cake formation, J. Membr. Sci. 239 (1) (2004) 39–53.
[25] C.C. Ho, A.L. Zydney, A combined pore blockage and cake filtration model for protein fouling during microfiltration, J. Colloid Interface Sci. 232 (2000) 389–399.
[26] W. Yuan, A. Kocic, A.L. Zydney, Analysis of humic acid fouling during microfiltration using a pore blockage-cake filtration model, J. Membr. Sci. 198 (2002) 51–62.
[27] J.E. Kilduff, S. Mattaraj, M. Zhou, G. Belfort, Kinetics of membrane flux decline: the role of natural colloids and mitigation via membrane surface modification, J. Nanopart. Res. 7 (2005) 525–544.
[28] N.R. Draper, H. Smith, Applied Regression Analysis, 3rd Edition, Wiley Interscience, 1998, ISBN 0-471-17082-8.
[29] J.E. Kilduff, S. Mattaraj, A. Wigton, M. Kitis, T. Karanfil, Effects of reverse osmosis isolation on reactivity of naturally occurring dissolved organic matter in physicochemical processes, Water Res. 38 (4) (2004) 1026–1036.
[30] C.N. Sawyer, P.L. McCarty, G.F. Parki, Chemistry for Environmental Engineering and Science, 5th ed. McGraw-Hill, NY, USA, 2003.
[31] A. Braghetta, F.A. DiGiano, W.P. Ball, Nanofiltration of natural organic matter: pH and ionic strength effects, J. Environ. Eng., ASCE 123 (7) (1997) 628–641.
[32] M.R. Teixeira, M.J. Rosa, M. Nystrom, The role of membrane charge on nanofiltration performance, J. Membr. Sci. 265 (2005) 160–166.